ORIGINAL PAPER

Similar Simulation Test of Overlying Rock Failure and Crack Evolution in Fully Mechanized Caving Face with Compound Roof

Wang Xiaolei

Abstract In the process of coal mining, the characteristics of overburden failure and the evolution of cracks were of great significance to the prevention and control of mine water and gas by using similar simulation test to study the overlying rock failure and crack evolution law of Yuwu Coal Industry's compound roof and large cutting height fully mechanized caving face. The results show that: the height of the caving zone is 32.6 m and the height of the fracture zone is 64.6 m; The influence of coal seam mining process on the supporting pressure of the roof overlying rock, the near seam was larger, the far seam was smaller; The inclination angle of the overburden mining fissures was medium angle, the width was mainly medium width, and the number of fissures gradually decreases as they move away from the coal seam; During the mining process, the overlying strata of the coal seams at a short distance are the gathering areas of mining cracks, and the density curve of the overlying cracks presents a "wave" shape.

W. Xiaolei (✉)
Department of Mining Engineering, Luliang University, No. 1, Xueyuan Road, Lishi District, Luliang City 033000, Shanxi Province, China
e-mail: 18039172835@126.com

1 Introduction

China is a large country in coal mines, and coal has an important role in economic development in my country (Huang et al. 2021; Li et al. 2020a; Wang et al. 2020a). Coal energy is closely related to our lives, and is an indispensable substance foundation for social and economic development (Zhang et al. 2021a; Wang et al. 2020b; Fu and Wang 2020). In my country's primary performance source structure, oil and natural gas storage is very small, in contrast (Zhao and Fu 2020; Wang et al. 2020c; Zhu et al. 2019; Cheng et al. 2020), the coal reserves are very large, although my country has vigorously developed new energy in recent years, but the status of coal energy main body will not change within a period of time (Zhu and Teng 2021; Zuo et al. 2019; Zhang et al. 2021a, 2019; Li and Wang 2020; Hu et al. 2020). "Energy Development Strategic Action Plan (2014–2020)" pointed out that by 2020 (Xu and Gao 2020; Yang et al. 2020a; Xia et al. 2020; Wang et al. 2020d; Ren 2020), the total energy consumption of energy consumption was around 4.8 billion tons of standard coal, and the total coal consumption was controlled around 4.2 billion tons, of which coal accounted for one energy proportion (Su et al. 2020; Wang 2019; Yang et al. 2020b; Xu et al. 2019). It is 62%. This can be seen that my country's energy or coal is mainly coal in a quite long time in the future

(Zhang et al. 2021a; Gao 2019; Chen et al. 2021; Li et al. 2021).

After the coal resource was taken, the coal seam of coal seams affected by the pilot field was called a moblite (Kang 2020; Jia and Hu 2020; Jiang et al. 2021). After the coal seam mining, the overclocking layer will have a movement, breaking phenomenon, and there is a fissure. The fracture can be divided into vertically breaking fracture, and the rock layer is alleviated by its nature (Zhang et al. 2020b, 2021a; Yu et al. 2021; Ma et al. 2020). The distribution of cracking fractures is not only important for mine water damage governance and the protection of water resources, but also has an important role in gas disaster prevention and coalbed methane resource development (Liu et al. 2020; Zhang et al. 2021b; Chen 2020; Cai 2020). Coal-grade top plate rocky "two bands" developmental height and the distribution of the fracture are very complex, and the geological characteristics of the coal-coating engineering, coal seam mining thickness and coal mining methods. Currently, the "two band" heights are more, there is formula method, material detectance, and drilling method (Bi et al. 2020; Wang et al. 2021; Qie et al. 2021; Pan et al. 2020). The "two band" calculation formula in the "Three Coal Regulations" is only applicable to coal seams that are thin and medium and thickly laminated, and it is not suitable for overall mining and high thick coal seams (Wang and Wang 2021; Li and Du 2020; Kang 2021; Gao 2021; Fu and Wang 2020).

Fully mechanized caving mining has become the main coal mining method for medium and thick coal seams in China (Cai et al. 2020; Zhang and Wang 2020; Li et al. 2020b). The complexity and dynamic invisibility of the overlying rock activity process during the mining of fully mechanized caving mining face brings difficulties to coal production, and similar simulation tests can be intuitive The whole process of overburden deformation (Hou et al. 2020; Fan 2020), movement and fracture during the mining process was one of the methods to deeply understand the failure and crack evolution of the overburden in fully mechanized caving mining, and can more accurately determine the "two zones" of the overburden after mining (Chai et al. 2020a; Chen et al. 2020). The development height and the evolution process of fissures provide important theoretical basis for mine

water disaster prevention and gas prevention (Zhang et al. 2021c; Chai et al. 2020b; Zhang et al. 2020a).

For the similar simulation study of overburden failure due to mining, Zhai (2002) simulated the movement of overburden under fully mechanized caving mining in Yima Changcun Coal Mine, studied the changes in the level of caving zone and fracture zone, and revealed the "masonry The "beam" structure develops towards high-rise level; Zhang and Hou (2007) conducted an experimental study on the movement of the roof of the first mining face in Nanliang Coal Mine, the compression strength, and the deformation and failure of the roadway, and summarized the overburden movement in the thick soil layer and shallow coal seam. The failure law, and proposed to strengthen the support to prevent the roof collapse in a large area, provides a necessary basis for the realization of the normal mining of thick soil layer and shallow coal seam.

The above-mentioned scholars have conducted similar simulation studies on the overburden rock caused by mining, mainly from the development height of the "two belts" of the overburden rock, the characteristics of surface movement, and the stress changes in the stope. However, there was no further study on the evolution of cracks during the advancement of the working face. Coal Mining S1202 working face was the test face, and similar simulation research was carried out on the height of the overlying rock "two zones", subsidence characteristics, stress field changes, and fracture evolution during mining.

2 Engineering Situation

The designed production capacity of Yuwu Coal Mine of Lu'an Group was 6Mt/a, and the main coal seam was 3#. The average thickness of the coal seam in the S1202 working face of the simulation test was 6.15 m, and the average mining depth was 412 m. It was a near-level coal seam and adopts fully mechanized caving mining. The mining ratio was 1:0.92. The working surface has four roadway, gas emission roadway, return airway, belt transportation, intake airway (the layout is shown in Fig. 1). Roof features: (1) The direct roof was sandy mudstone with a thickness of about 5.65 m; (2) The basic roof was fine-grained sandstone and siltstone with a thickness of about 11.2 m, and there are staggered joints.
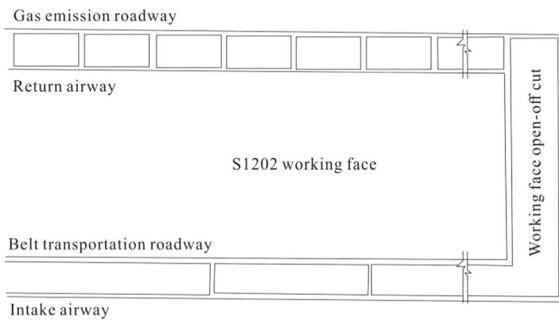
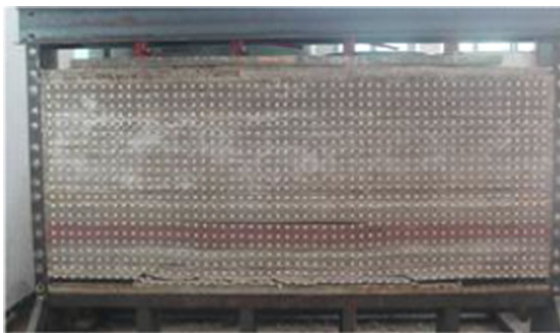**Fig. 1** Layout of working face

3 Similarity Simulation Experiment

3.1 Test Equipment

According to the purpose of this test, a stress test bench was used, the size of the test bench was 3300 mm × 1800 mm × 300 mm (length × width × height), as shown in Fig. 2, and the rock mechanics parameters are shown in Table 1.

3.2 Proportional Similarity

According to the similarity test principle and the actual situation of the S1202 working face, the similarity ratio was determined, and the details are as follows:

(1) Geometric similarity coefficient: $C_l = L_M/L_H = 1/200$, Among them, C_l was the geometric similarity ratio, L_M and L_H are the length of the model and prototype respectively.

(2) Time similarity coefficient: $C_t = T_M/T_H = \sqrt{C_l} = 1 : 14.1$, In order to accurately grasp the time during excavation, take 1/12, where C_t

was the time similarity ratio, T_M was the model process time, and T_H was the prototype process time.

(3) Similarity coefficient of bulk density: $C_\gamma = \gamma_M/\gamma_H = 3 : 5$, Among them, C_γ was the bulk density similarity ratio, γ_M model bulk density, and γ_H prototype bulk density.

(4) Similarity coefficient of elastic modulus: $C_E = E_M/E_H = C_l C_\gamma = 3/1000$, Among them, C_E was the elastic modulus similarity ratio, E_M was the model elastic modulus, and E_H was the prototype elastic modulus.

(5) Strength similarity coefficient: $C_\sigma = \sigma_M/\sigma_H = C_l C_\gamma$, Among them, C_σ was the uniaxial compressive strength similarity ratio, σ_M was the model uniaxial compressive strength, and σ_H was the prototype uniaxial compressive strength.

The test model uses fine sand as aggregate and gypsum and lime as cementing materials. According to the similarity ratio, the physical and mechanical parameters of the similar model and the ratio of similar materials are shown in Tables 2 and 3.

3.3 Observation Point Arrangement and Observation Method

The displacement and stress measuring point layout was shown in Fig. 3.

Four effective displacement observation lines and one stress observation line are arranged in the overburden of the coal roof. The displacement line observes the breakage of the overburden of the coal roof, and the stress line observes the change of the overburden stress during the mining process. In the experiment, an electronic total station was used to observe the displacement line.

Electronic total station is a high-tech measuring instrument integrating lighting, machine, and electricity. It is a synthetic angle, vertical angle, distance, high-profile measurement function in a surveying instrument system. Comparing the optical coiler to compare the electropolite to the photoelectric scanning disc, the artificial optical micrograph generation is automatically recorded and displayed, so that the angular operation is simplified, and the generation of reading errors can be avoided. All measurement work

Fig. 2 Station of similar simulation test

Table 1 Rock mechanics parameters

Rock type	Density (g·cm^{-3})	Compressive strength (MPa)	Elastic modulus (GPa)	Cohesion (MPa)	Internal friction angle (°)	Poisson ratio
Medium sandstone	2.69	62.0	7.6	2.7	34	0.33
Mudstone	2.31	49.3	6.3	2.2	31	0.31
Fine sandstone	2.42	58.1	6.4	2.4	33	0.30
Siltstone	2.61	35.2	5.6	2.6	35	0.32
Coal	1.41	10.6	1.4	1.1	19	0.34

Table 2 Physico-mechanical parameters of similar model

Rock type	Density (g·cm^{-3})	Compressive strength (MPa)	Elastic modulus (GPa)	Cohesion (MPa)	Internal friction angle (°)	Poisson ratio
Medium sandstone	1.61	0.27	7.6	0.008	34	0.33
Mudstone	1.39	0.13	6.3	0.007	31	0.31
Fine sandstone	1.45	0.22	6.4	0.007	33	0.30
Siltstone	1.57	0.21	5.6	0.007	35	0.32
Coal	0.85	0.03	1.4	0.003	19	0.34

Table 3 Similar materials ratio of test

Rock type	Similar material and ratio
Medium sandstone	Fine sand:Lime:Gypsum:Water = 10.1:1.0:2.3:1.94
Mudstone	Fine sand:Lime:Gypsum:Water = 11.1:1.0:1.0:1.40
Fine sandstone	Fine sand:Lime:Gypsum:Water = 13.1:1.0:2.3:1.8
Siltstone	Fine sand:Lime:Gypsum:Water = 13.6:1.0:2.6:2.1
Coal	Fine sand:Lime:Gypsum:Water = 5.90:1.0:1.0:1.1
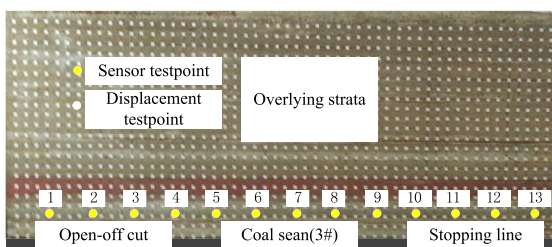
Fig. 3 Measuring points layout of displacement and stress

on the station can be completed due to its resettlement instrument.

Its test principle is to provide a spectroscopic prism system between the telephoto objective and the focus lens, and the multi-function of the telescope is achieved by the system, that is, aiming at the target, making it imaged on a cross wire plate, angular measurement, and it is measured The outer light path system of the distance can also cause a modulated infrared light emitted by the photosensitive diode of the ranging portion to the reflective prism in the substrate lens. Reflected by the same path, then the substantial prism is used to receive the backlight by the photodiode, and the ranging needs to have another inner optical path system inside the instrument, and the optical fibers in the spectroscope system will be transmitted by the photodiode. Infrared light transmission also given to the photodiode reception,

performing the phase difference between the inner and outer light path modulated light, calculates the propagation time, calculating the measured distance.

Yuwu Coal Industry S1202 face production was 9 cuts per day, and each cut was 0.8 m. According to the time similarity ratio, the model simulates the actual coal intake of 1.8 cm/h.

4 Test Process and Analysis of Results

4.1 "Two Zones" Damage Height

Figure 4 shows the development process of overlying strata "two zones" during the mining process of the working face. After the working face was mined, the overlying rock near the coal wall begins to move. When the working face advances 90 m, the old roof breaks for the first time and the overlying rock was separated; when the working face advances to 120 m, the old roof collapses for the first time and its covering Rock fissures are developed; when the working face advances to 190 m, the goaf was gradually compacted

and the pressure rises; when the working face advances to 240 m, the middle of the goaf was completely compacted, the cracks are closed, and a sinking basin was formed. According to the histogram of S1202 working face of Yuwu Coal Industry, the dynamic development height of the overlying rock "two zones" was shown in Table 4.

4.2 Analysis of the Highest Fracture Location and Collapse Height

For the prevention and control of mine water and gas disasters, it was necessary not only to study the distribution of the overburden fissure field during mining, but also to study the overburden collapse of the coal seam roof and the dynamic changes of the separation height during the advancement of the working face, so as to achieve a comprehensive understanding of the mining face The evolution of the cracks and the gas migration and accumulation patterns in the process. Figure 5 shows the relationship between the advancing distance of the working face and the highest position of the crack and the height of the collapse.

It can be seen from Fig. 4 that the development of separation cracks and broken fractures are not completely synchronized with the rock movement, and they develop nonlinearly from bottom to top. The separated cracks develop faster than broken fractures. When the working face advances to about 170 m, the cracks develop the height of the coal seam was about 75 m. Every time the working face advances by 6–10 m on average, the range of the overlying strata will increase, and the position of the overlying strata will increase, and the breakage and collapse of the coal roof overlying strata are particularly obvious.

4.3 The Deformation Law of Overlying Strata in Stope

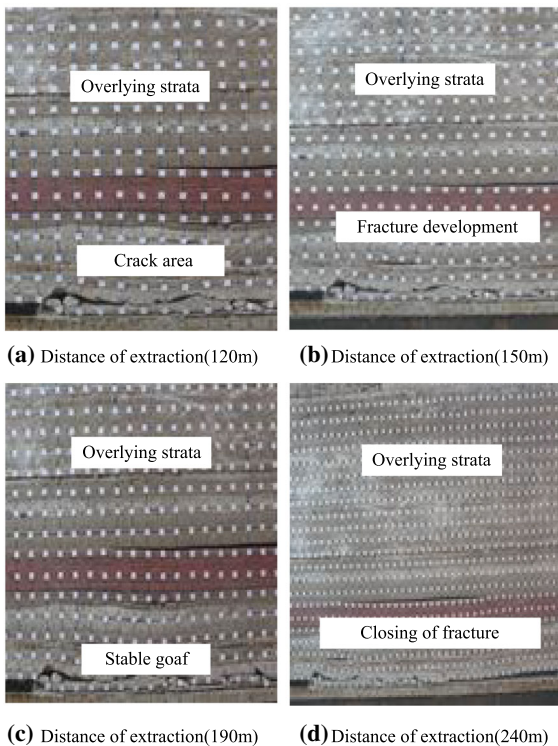In order to visually analyze the movement and deformation laws of the overburden strata of the

(a) Distance of extraction(120m) **(b)** Distance of extraction(150m)

(c) Distance of extraction(190m) **(d)** Distance of extraction(240m)

Fig. 4 The roof falling shape of different advance distance

Table 4 Development height of two zones of overburden

Name	Failure height (m)
Caving zone	32.6
Fractured zone	64.6
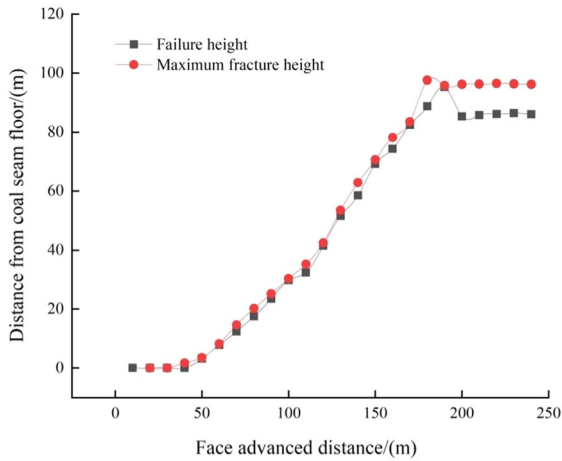
Fig. 5 The relationship among fissure and falling height and the advance distance

stope, the advancement distance of the working face and the movement variation of the overburden strata are placed in the same coordinate system, and the variation curve of the displacement variation with the working face was shown in Fig. 6.

From Fig. 6, the subsidence curve of the overlying strata at different advancing distances shows that the overlying strata was in a state of original stress balance when the coal seam was not mined. When coal resources are mined, the overlying strata above the goaf undergoes elasticity to shape The state changes, with the continuous advancement of the working face,

the overlying strata moves, breaks and collapses, forming the "three zones" of the overlying strata (breakdown zone, fissure zone, and bending subsidence zone), and the subsidence of the overburden strata was nonlinear, Movement was asymmetry; due to the different strengths, thicknesses, bedding development, and joint development of each layer of the overburden, the movement and movement of each rock layer are asynchronous, and the group movement characteristics of the key layers are mainly coordinated. With the advancement of the working face, the development height of the overburden caving zone and fissure zone gradually rises. When the working face advances for a certain distance, the height remains basically unchanged. The overburden (except the caving zone) experienced during coal mining a continuous and dynamic process of sinking and moving. The movement of the far coal seam was more obvious, and the movement curve shape was similar to that of the ground. The near-coal rock layer, when the overburden straddles, the sinking curve was more irregular.

4.4 Stress Distribution of Overlying Strata in Stope

During the advancing process of the working face, the stress of the overburden rock mass of the coal seam roof goes through three stages of pressure increase before mining, pressure relief after mining, and

(a) Distance of mining(140m)
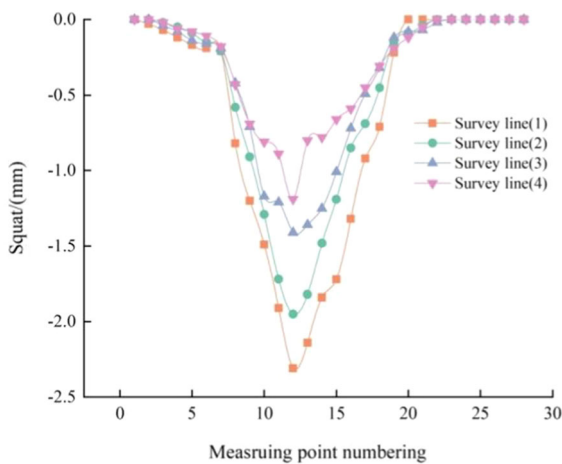

(b) Distance of mining(240m)
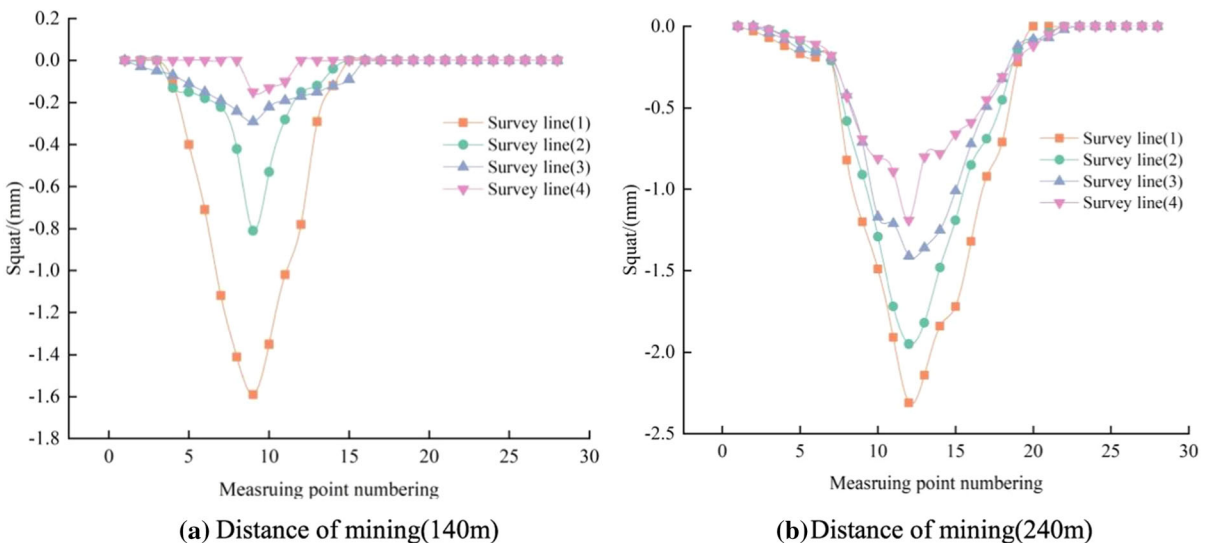
Fig. 6 Sinking curve of different advance distance

pressure stabilization recovery. The observation of the stress of the roof overburden reveals the behavior of the stress in the goaf during the mining process. The overburden failure characteristics, the supporting pressure distribution curve when the working face was mined at 90 m and 240 m are shown in Fig. 7.

It can be seen from the Fig. 7 that during the coal mining process, the abutment pressure has a larger range of influence, with a higher peak value. The peak value was 75 m away from the working face. The stress was lower in the range of 0–50 m behind the working face, forming a stress reduction zone. The stress rises slowly in the range of 50–100 m behind the working face, forming a stable zone of supporting pressure, because the gangue was gradually compacted by the roof. Under different mining depths, the greater the mining depth, the smaller the concentration of support pressure. Because the surrounding rock was fractured and softened under high stress, the high-stress area becomes wider, and the internal stress field becomes wider with the increase in mining depth.

5 Quantitative Analysis of Fracture Development of Mining Overburden

Mining fissures are not only of great significance for mine water disasters and water resources protection, but also play an important role in gas disaster prevention and coalbed methane development. Therefore, the inclination, width, number and height of overburden cracks are quantified after they are fully mined. According to analysis, Fig. 8 shows a developed crack in the overlying rock after mining.

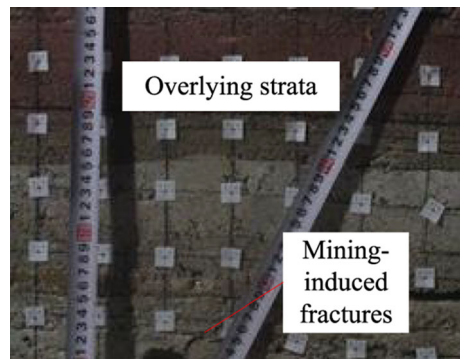### 5.1 Distribution of Fracture Dip Angle

After fully mining, there are 34 mining fissures in the entire overburden, with different inclination angles of the fissures. Figure 9 shows the distribution curve based on the inclination of the fissures.

It can be seen from the distribution curve of fracture dip angle and quantity in Fig. 9 that among the 34 fractures after fully mining, 6 fractures with dip angle less than 30 account for 17.65% of all fractures, 8 fractures with dip angle of 30–39 account for 23.53% of all fractures, and 9 fractures with dip angle of 40–49 account for 26.47% of all fractures with dip angle of 50 It accounts for 11.76% of all fractures, including 2 fractures with dip angle of 60–69, 5.880%, 3 fractures with dip angle of 70–79, 8.830%, and 2 fractures with dip angle of 80–90, accounting for 5.880% of all fractures.

5.2 Distribution of Crack Width

The crack width reflects the degree of crack development. Under mining, the crack development width near the coal seam was larger. Figure 10 shows the distribution curve based on the crack width.

Figure 10 shows that there are 6 cracks with width less than 1 mm, accounting for 17.65% of all cracks, 9 cracks with width of 1–1.9 mm, accounting for 26.47%, 11 cracks with width of 2–2.9 mm, accounting for 32.35% of all cracks, and 7 cracks with width of 3–3.9 mm, accounting for 20.59% of all cracks.

Fig. 7 Abutment pressure distribution cures different advance distance

**Fig. 8** Mining-induced fractures under overburden
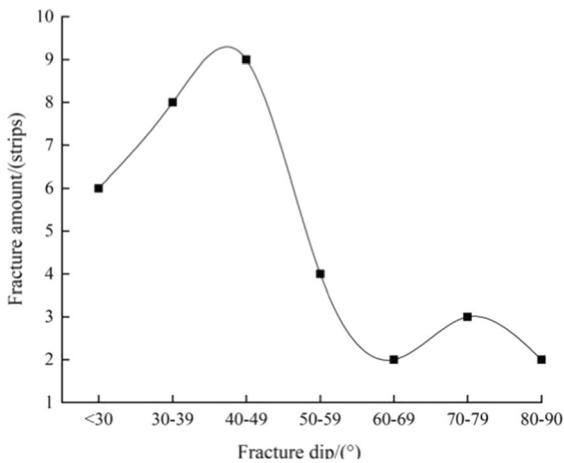
Fig. 9 Dip angle distributions of fissure

5.3 Number of Fractures and Overburden Height

The change characteristics of the height of the overburden and the number of fractures reflect the degree of the overburden affected by mining. Figure 11 shows the relationship between the number of mining cracks and the height of the overlying strata.

It can be seen from Fig. 11 that the coal seams at close distances are greatly affected by mining, so there are a large number of cracks, which are mainly concentrated in the overburden about 90 m.
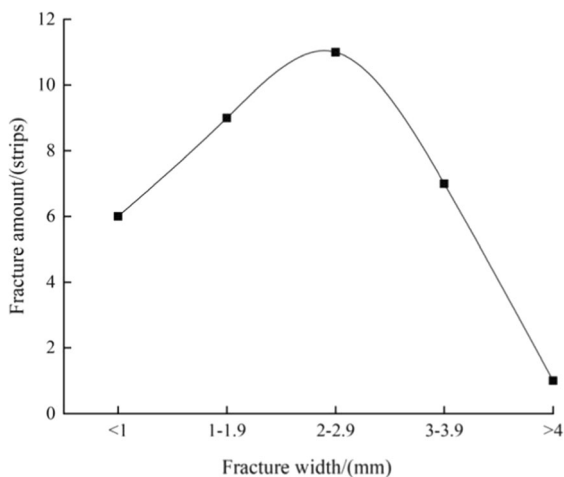
**Fig. 10** Distributions of fracture width
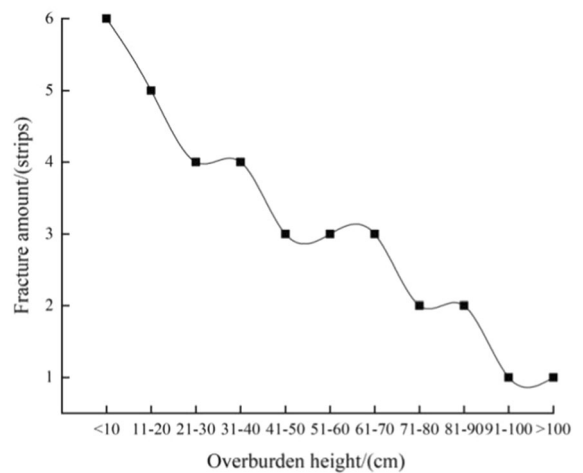
Fig. 11 Relationship curves between overburden height and quantity of fractures

5.4 Distribution of Mining Fractures

In order to visually describe the development of mining fractures, the fracture density (bars/m) was used to represent the development of fractures. According to the experimental data, the curve of fracture density at different advance distances was shown in Fig. 12.

Figure 12 shows the crack density distribution curve of the overburden: during the mining process, the overburden moves, breaks, collapses, and develops into three stages:

(1) Within about 60 m, the roof overburden changes from elastic deformation to plastic deformation, failure and instability until the cracks transition, the number and width of the cracks increase simultaneously in the process.
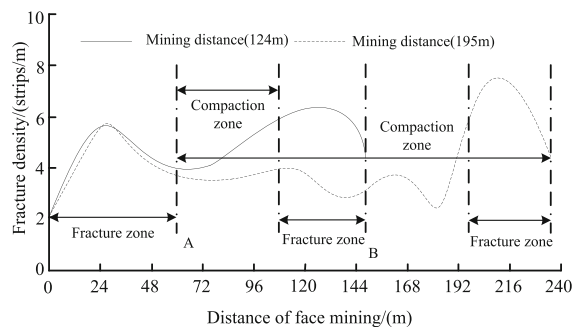
Fig. 12 Distribution law of overlying fissure density

(2) With the continuous advancement of the working face, the mining fissures develop to the high level. When pushed to a certain distance, the mined-out area was compacted by the roof overlying rock, and the density decreases rapidly.

(3) In the area near the coal wall, due to the supporting effect, the crack density was still high.

6 Conclusions

(1) A similar simulation study was carried out on a fully mechanized caving mining face with large mining height and composite roof of Yuwu Coal Industry, and it was concluded that the height of the caving zone was 32.6 m and the height of the fracture zone was 64.6 m.

(2) The width of the mining cracks in the overburden of the coal seam roof was mainly medium width, and the inclination angle was mainly the middle angle, and the number of cracks gradually decreases with distance from the coal seam. In this area, the density curve of overlying rock fractures was in a "wave" shape.

Data Availability Data will be made available on reasonable request.

References

Bi YL, Li XL, Guo N (2020) Spatial heterogeneity of vegetation and soil nutrients induced by the open-pit mining in eastern grassland of China. J Min Strat Control Eng 2(4):047036

Cai MF (2020) Key theories and technologies for surrounding rock stability and ground control in deep mining. J Min Strat Control Eng 2(3):033037

Cai YF, Li XJ, Deng WN, Xiao W, Zhang WK (2020) Simulation of surface movement and deformation rules and detriment key parameters in high-strength mining. J Min Strat Control Eng 2(4):043511

Chai J, Ou YYB, Zhang DD (2020a) Crackdetection method in similar material models based on DIC. J Min Strat Control Eng 2(2):023015

Chai J, Ou YYB, Zhang DD, Lei WL (2020b) Theoretical analysis of the mechanical coupling between rock and optical fiber for distributed sensing of overlying strata deformation. J Min Strat Control Eng 2(3):033038

Chen JW (2020) Analysis of roadheader's rotary table on vibration modal based on finite element method and tested data. J Min Strat Control Eng 2(2):026032

Chen SL, Huang BX, Li D, Zhao XL, Xu J, Wang CW (2020) Experiment study on the basic law of high pressure abrasive hydraulic cutting for coal-rock mass. J Min Strat Control Eng 2(4):047521

Chen J, Gao JK, Pu YY, Jiang DY, Qi QX, Wen ZJ, Sun QL, Chen LL (2021) Machine learning method for predicting and warning of rockbursts. J Min Strat Control Eng. 3(1):013026

Cheng JW, Zhao G, Sa ZY, Zheng WC, Wang YG, Liu J (2020) Overlying strata movement and deformation calculation prediction models for underground coal mines. J Min Strat Control Eng 2(4):043523

Fan K (2020) Sudden deformation characteristic and cutting-roof support technology for double-used roadways in Longtan Mine. J Min Strat Control Eng 2(3):033032

Fu X, Wang RF (2020) Cooperative self-adaptive control model of fluid feeding system and hydraulic supports in working face. J Min Strat Control Eng 2(3):036031

Gao FQ (2019) Use of numerical modeling for analyzing rock mechanic problems in underground coal mine practices. J Min Strat Control Eng 1(1):013004

Gao FQ (2021) Influence of hydraulic fracturing of strong roof on mining-induced stress-insight from numerical simulation. J Min Strat Control Eng 3(2):023032

Hou EK, Cong T, Xie XS, Wei JB (2020) Ground surface fracture development characteristics of shallow double coal seam staggered mining based on particle flow. J Min Strat Control Eng 2(1):013521

Hu QF, Cui XM, Liu WK, Ma TJ, Geng HR (2020) Law ofoverburden and surface movement and deformation due to mining super thick coalseam. J Min Strat Control Eng 2(2):023021

Huang FR, Yan SX, Wang XL, Jiang PC, Zhan SB (2021) Experimental study on infrared radiation characteristics of gneiss under uniaxial compression. J Min Strat Control Eng. 3(1):013011

Jia C, Hu CC (2020) Instability mechanism and control technology of longwall entries driving along the gob in a thick coal seam. J Min Strat Control Eng 2(4):043535

Jiang KG, Wang L, Chi SS, Wei T, Jiang C (2021) Boltzmann function prediction model coupled with the correction of inflection point offset and its parameter inversion method. J Min Strat Control Eng 3(2):023527

Kang HP (2020) Spatial scale analysis on coalmining and strata control technologies. J Min Strat Control Eng 2(2):023538

Kang HP (2021) Temporal scale analysis on coal mining and strata control technologies. J Min Strat Control Eng. 3(1):013538

Li Y, Du G (2020) Reasonable width of narrow coal pillars in roadway driving with gas drainage hole. J Min Strat Control Eng 2(1):013007

Li JK, Wang H (2020) Ground support of interbedded rock roof in a deep roadway with fully-anchored cables. J Min Strat Control Eng 2(3):033036

Li JH, Li HJ, Li ZC, Wu ZQ (2020a) Research on river dike failure of short-distance coal seams mining under Hunchun River. J Min Strat Control Eng 2(1):013538

Li YP, Cui F, Yang WH, Wei CXQ (2020b) Dynamic migration law and its control of roof in fully mechanized top coal caving mining in extremely steep and thick coal seams. J Min Strat Control Eng 2(4):043538

Li JY, Wang L, Jiang KG, Teng CQ (2021) Parameter inversion method of probability integral model based on improved wolves algorithm. J Min Strat Control Eng. 3(1):017038

Liu YX, Gao MS, Zhao HS, He SL, Li ZG, Zhang ZC (2020) Detection of overlying rock structure and identification of key stratum by drilling and logging technology. J Min Strat Control Eng 2(2):023038

Ma WZ, Zhou XM, Tan S (2020) Study on failure characteristics of coal seam floor above confined water: a case study of Shanxi Yitang Coal Mine. J Min Strat Control Eng 2(3):033011

Pan H, Zhu L, Zhang XF, Gu WZ, Liu ZC, Li J, Song TQ, Qiu FQ (2020) Distribution characteristics of deviatoric stress and control technology of surrounding rock at temporary water chamber group in deep mining. J Min Strat Control Eng 2(4):043033

Qie L, Shi YN, Liu JG (2021) Experimental study on grouting diffusion of gangue solid filling bulk materials. J Min Strat Control Eng 3(2):023011

Ren YF (2020) Analysis and evaluation method for supporting ability of supports in coalmine working face. J Min Strat Control Eng 2(3):036012

Su SL, Du Y, Zhu JF, Zhang L, Zhao ZL, Meng B (2020) Numerical study on bearing behavior of layered rock mass for deep roadway. J Min Strat Control Eng 2(1):013002

Wang JC (2019) Sustainable coal mining based on mining ground control. J Min Strat Control Eng 1(1):013505

Wang J, Wang XL (2021) Seepage characteristic and fracture development of protected seam caused by mining protecting strata. J Min Strat Control Eng. 3(3):033511

Wang GF, Pang YH, Ren HW (2020a) Intelligent coal mining pattern and technological path. J Min Strat Control Eng 2(1):013501

Wang J, Zhang C, Zheng D, Song WD, Ji XF (2020b) Stability analysis of roof in goaf considering time effect. J Min Strat Control Eng 2(1):013011

Wang P, Zhang BS, Wang L, Lin XY, Song XF, Guo JQ (2020c) Research on roof falling mechanism and support technology of mining roadway in expansive soft rock. J Min Strat Control Eng 2(2):023022

Wang Y, Tu M, Fu BJ, Bu QW (2020d) Lateral mining-induced stress distributive property of deep mining and gob-side entry support. J Min Strat Control Eng 2(3):033012

Wang DL, Hao BY, Liang XM (2021) Slurry diffusion of single fracture based on fluid-solid coupling. J Min Strat Control Eng. 3(1):013038

Xia YX, Lu C, Yang GY, Su SJ, Pang LN, Ding GL, Su B (2020) Experimental study on axial fracture cutting and fracturing of abrasive jet in hard roof hole. J Min Strat Control Eng 2(3):033522

Xu NZ, Gao C (2020) Study on the special rules of surface subsidence affected by normal faults. J Min Strat Control Eng 2(1):011007

Xu JL, Xuan DY, Zhu WB, Wang XZ (2019) Partial backfilling coal mining technology based on key strata control. J Min Strat Control Eng 1(1):013504

Yang DF, Zhang YJ, Wang S, Niu CH, Chai JL (2020a) Analysis of the influence of hidden fault dip angle on ground pressure behavior in shallow seam roof. J Min Strat Control Eng 2(4):043038

Yang GH, Wang K, Zhang XQ (2020b) Study on non-pillar mining technology of preset packing body and roof cutting in deep well roadway. J Min Strat Control Eng 2(1):013038

Yu XY, Wang ZS, Yang Y, Mao XW (2021) Numerical study on the movement rule of overburden in fully mechanized caving mining with thick depth and high mining height. J Min Strat Control Eng 3(1):013533

Zhai XX (2002) Study of strata movement face roof based on similar simulation in full-mechanized top coal caving faces. J Rock Mech Eng 21(11):1667–1671

Zhang J, Hou ZJ (2007) Failure rule of overburden movement in shallowly buried coal seam covered with thick soils. J Min Saf Eng 24(1):56–59

Zhang T, Wang YL (2020) Study on deformation evolution law and support technology of surrounding rock in multiple mining roadway. J Min Strat Control Eng 2(2):023016

Zhang N, Han CL, Xie ZZ (2019) Theory of continuous beam control and high efficiency supporting technology in coal roadway. J Min Strat Control Eng 1(1):013005

Zhang BL, Shen BT, Zhang JH, Zhang XG (2020a) Experimental study of edge-opened cracks propagation in rock-like materials. J Min Strat Control Eng 2(3):033035

Zhang C, Song WD, Fu JX, Li Y, Zhang KC (2020b) Technology for roadway management of fractured rock masses in a submarine gold mine. J Min Strat Control Eng 2(3):033039

Zhang GJ, Yan W, Jiang KG (2021a) Inversion method for the prediction parameters of mining subsidence based on the PB combination prediction model of variable weight. J Min Strat Control Eng. 3(1):013524

Zhang KX, Wang XL, He MC, Yin SX, Li SB, Sun JD, Li D, Cheng ZH, Zhao QF, Yin SF, Kang L, Zhu JA, Yang HJ (2021b) Research on multi-level fuzzy comprehensive evaluation of the applicability of intelligent unmanned mining face. J Min Strat Control Eng. 3(1):013532

Zhang XF, Qu XC, Wei QD (2021c) Development and application of multi-dimension multi-parameter monitoring and early warning platform of coal bursts. J Min Strat Control Eng. 3(1):013013

Zhao QC, Fu BJ (2020) Study on loose zone testing and support technology of roadway surrounding rock affected by dynamic pressure. J Min Strat Control Eng 2(2):023031

Zhu W, Teng YH (2021) Study on the safety and mining influence of fully-mechanized caving mining with ultra-thick seam under barrier lake. J Min Strat Control Eng. 3(1):013525

Zhu WC, Niu LL, Li SH, Li S (2019) Creep-impact test of rock: status-of-the-art and prospect. J Min Strat Control Eng 1(1):013003

Zuo JP, Yu ML, Hu SY, Song HQ, Wei X, Shi Y, Zuo SH (2019) Experimental investigation on fracture mode of different thick rock strata. J Min Strat Control Eng 1(1):013007